Main-Group Chemistry Hot Paper

How to cite: *Angew. Chem. Int. Ed.* **2022**, *61*, e202211749
International Edition: doi.org/10.1002/anie.202211749
German Edition: doi.org/10.1002/ange.202211749

A Germapyramidane Switches Between 3D Cluster and 2D Cyclic Structures in Single-Electron Steps

Peter Coburger, Fabio Masero, Jonas Bösken, Victor Mougel,* and Hansjörg Grützmacher**

Dedicated to Guy Bertrand on the occasion of his 70th birthday

Abstract: Reaction of the imidazolium-substituted iphosphate-diide, $(Ipr)_2C_2P_2$ (**IDP**), with $GeCl_2\cdot$dioxane and $KBArF_{24}$ [$(BarF_{24})^-$ = tetrakis[(3,5-trifluoromethyl)phenyl]borate)] afforded the dicationic spherical-aromatic *nido*-cluster $[Ge(\eta^4\text{-}\mathbf{IDP})]^{2+}$ ($[\mathbf{1}]^{2+}$) (Ipr = 1,3-bis(2,6-diisopropylphenyl)imidazolium-2-ylidene). This complex is a rare heavy analogue of the elusive pyramidane $[C(\eta^4\text{-}C_4H_4)]$. $[\mathbf{1}]^{2+}$ undergoes two reversible one-electron reductions, which yield the radical cation $[\mathbf{2}]^{\bullet+}$ and the neutral Ge^{II} species **3**. Both $[\mathbf{2}]^{\bullet+}$ and **3** rearrange in solution forming the 2D aromatic and planar imidazolium-substituted digermolide $[\mathbf{4}]^{2+}$ and germole-diide **5**, respectively. Both planar species can be oxidized back to $[\mathbf{1}]^{2+}$ using $AgSbF_6$. These redox-isomerizations correspond to the fundamental transformation of a 3D aromatic cluster into a 2D aromatic ring compound upon reduction and vice versa. The mechanism of these reactions was elucidated using DFT calculations and cyclic voltammetry experiments.

Introduction

As pointed out by Canac and Bertrand, the mutual conversion of a three-dimensional cluster with n-vertices into a planar aromatic ring compound is a transformation of fundamental interest in molecular chemistry.[1] This profound structural change is promoted by the addition/removal of an electron pair and as such links two fundamental concepts after those a valence electron count (VEC) is correlated with a specific molecular structure, namely the Hückel-rules for planar aromatic and anti-aromatic rings and the Wade-Mingos-Rudolph rules for clusters with triangular faces and n-vertices [the latter is also referred to as polyhedral skeletal electron pair theory (PSEP)].[2–4] This is illustrated in Scheme 1 for the smallest possible *closo*-cluster with $n = 5$ vertices and a trigonal bipyramidal structure. Addition of an electron pair converts *closo*-**A** [6 valence electron pairs (VEP)] either to *nido*-**B** [7 VEP] or the 2D anti-aromatic cycle **C** (two VEPs constitute the anti-aromatic 4π-electron system, five VEPs the ring sigma bonds). Further addition of an electron pair, transforms *nido*-**B** either to *arachno*-**D** [8 VEP] or the five membered aromatic ring **E**. An example from classical organic chemistry is found in the two-electron redox couple $[C_5R_5]^+ + 2e \rightleftharpoons [C_5R_5]^-$. While the ring $[C_5R_5]^-$ is doubtlessly a 2D aromatic compound in accord with the Hückel-rules,[5]

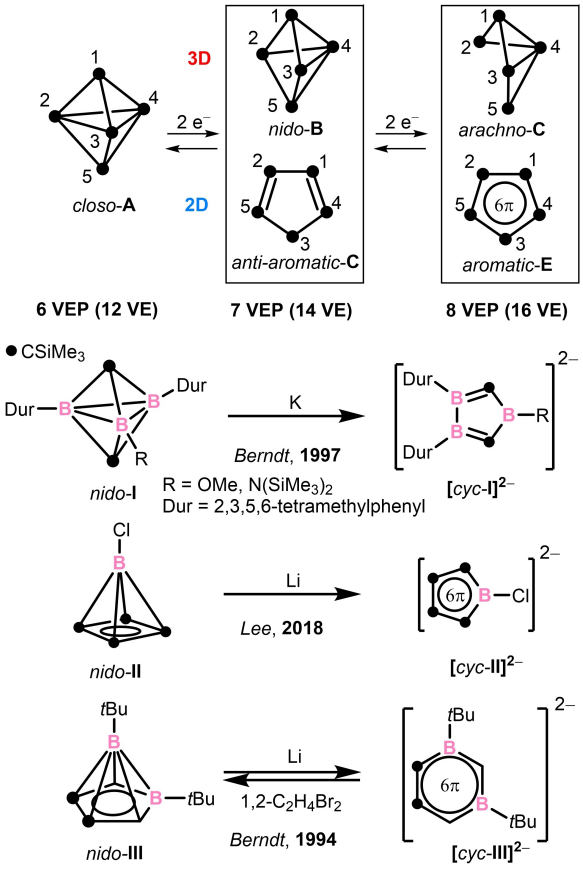

Scheme 1. Possible structural changes of a 5-vertex *closo*-cluster upon reduction and redox chemistry of carboranes *nido*-**I**, *nido*-**II** and *nido*-**III**.

[*] P. Coburger, F. Masero, J. Bösken, V. Mougel, H. Grützmacher
Department of Chemistry and Applied Biosciences, ETH Zürich
Vladimir-Prelog-Weg 1–5/10, 8093 Zürich (Switzerland)
E-mail: pcoburger@inorg.chem.ethz.ch
mougel@inorg.chem.ethz.ch
hgruetzmacher@ethz.ch

isolable $[C_5R_5]^+$ species remain elusive,[6–8] and may not show the square-pyramidal structure of a *nido*-cluster **B** predicted by the PSEP theory.[2–4]

In only three cases **I**,[9] **II**,[10] and **III**[11] (Scheme 1), a two-electron redox reaction allowed to convert a n-vertex cluster into a n-membered ring (other examples are known but here both partners of this formal two-electron redox pair were synthesized on independent synthetic routes; see the Supporting Information, Figure S1 for a list). And only for **III**, the reversibility of the chemical redox process was shown.

Formally the processes displayed in Scheme 1 require the simultaneous addition or removal of two electrons. But to our knowledge, the transfer of an "electron pair" has never been proven and is highly debated.[12] Much more likely are stepwise one electron transfers and, consequently, there must be intermediates along possible reaction paths, but these are currently unknown.

In this article we report the reversible conversion of a 5-vertex cluster into an aromatic 5-membered cycle. This process proceeds in consecutive one-electron redox steps and most intermediates were experimentally characterized. This allows finally to propose reaction mechanisms for the fundamental redox-promoted rearrangement of polyhedral 3D clusters into cyclic π-electron conjugated 2D cycles.

Results and Discussion

We assessed the 5-vertex *nido*-cluster $[\mathbf{1}](BArF_{24})_2$ by reacting the bis(imidazolium)-1,3-diphosphete-diide (**IDP**)[13] first with $GeCl_2$·dioxane and subsequently with two equivalents of $K(BArF_{24})$ (Scheme 2(a)). The product $[\mathbf{1}](BArF_{24})_2$ forms pale yellow crystals in 54 % yield after recrystallisation from 1,2-difluorobenzene (DFB)/hexane. The dication $[\mathbf{1}]^{2+}$ is a heavy analogue of the elusive pyramidane $[C\{\eta^4\text{-}(C_4H_4)\}]$[14–16] and is thus best described as a

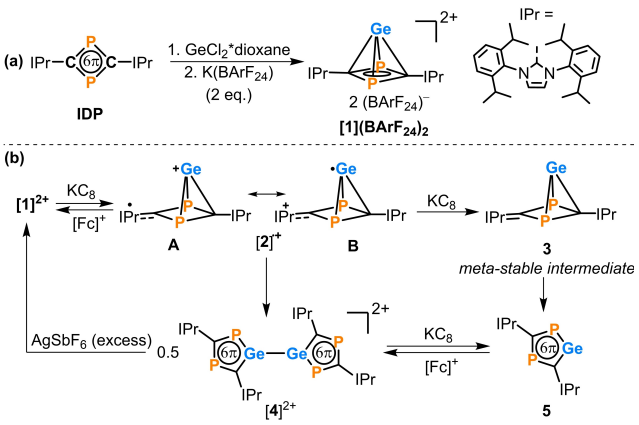

Scheme 2. Synthesis of $[\mathbf{1}](BArF_{24})_2$ (a); Synthesis of $[\mathbf{2}](BArF_{24})$·K$(BArF_{24})$, $[\mathbf{4}](BArF_{24})_2$·$K(BArF_{24})_{1.8}$ and **5**·$K(BArF_{24})$ (b). The counter anion for all cations in b) is $(BArF_{24})^-$. $[Fc]^+ = [Fe(Cp)_2]^+$ (ferrocenium). For clarity, in this and all following figures and schemes, an IPr group with a single bond to a C_2P_2 ring denotes a cationic imidazolium group.

germapyramidane. Alternatively, the reaction can be performed in presence of $GaCl_3$ as chloride abstracting reagent which allows to isolate single crystals of the composition $[\mathbf{1}](Ga_2Cl_7)(Ga_3Cl_{10})$ which were subjected to an X-ray diffraction analysis in order to determine its solid state structure. A plot of the dication $[\mathbf{1}]^{2+}$ is shown in Figure 1a.[17] Within the experimental errors, the central GeC_2P_2 pyramid in $[\mathbf{1}]^{2+}$ has two equal Ge–P bonds (Ø 2.447 Å) and two equal Ge–C bonds (Ø 2.273 Å) which are—as expected for pyramidanes[18–22,10] - elongated with respect to standard Ge–C (1.95–2.00 Å) and Ge–P (≈2.3 Å) single bonds.[23] The four equal P–C bonds (Ø 1.808 Å) fall within the expected range.[24] The relatively long C1–C3/C2–C4 bonds [1.441(3) Å *vs.* 1.38 Å in **IDP**] between the C_2P_2 ring and the exocyclic IPr groups (IPr = 1,3-bis(2,6-diisopropylphenyl)imidazolium-2-ylidene) indicate C–C single bond character and therefore the IPr units are best described as cationic imidazolium groups. Consequently, in accordance with DFT calculations (see the Supporting Information, section 9) and the classical electron-counting rules given above, $[\mathbf{1}]^{2+}$ can be formulated as a 5-vertex *nido*-cluster with seven skeletal electron pairs (the total valence electron count is given by: VEC = 4(Ge) + 2×5(P) + 2×4(C) + 2×2 (IPr) − 2 (positive charge) = 24 e; of these 2e/cluster atom = 10 e are used for external lone pairs (Ge, 2× P) or bonds (2× C-Ipr$^+$), which leaves 14 e ≙ 7 VEP for the *nido*-cluster). In the $^{31}P\{^1H\}$ NMR spectrum (CD_2Cl_2 solution) $[\mathbf{1}](BArF_{24})_2$ shows a singlet resonance at δ = 127.1 ppm while the ^{13}C nuclei of the central C_2P_2 ring are observed as a triplet at δ = 102.1 ppm ($^1J_{CP}$ = 50 Hz) in the $^{13}C\{^1H\}$ NMR spectrum. These data are comparable to the ones reported for the related neutral germapyramidane [Ge{η^4-*t*Bu$_2$C$_2$P$_2$}] ($^{31}P\{^1H\}$: δ = 142.2 ppm, $^{13}C\{1H\}$: δ = 124.2 ppm, $^1J_{CP}$ = 47 Hz).[19] A calculation of the Nuclear Independent Chemical Shift (NICS) in the center of the pyramid scaffold of $[\mathbf{1}]^{2+}$ (NICS = −22.5) together with a NICS-scan curve indicates spherical/3D aromaticity comparable to other pyramidane derivatives and the aromatic *nido*-cluster $(C_2B_9H_{12})^-$ (see the Supporting Information, section 9.2).[25,26] In addition, the electron localization function (ELF) of the valence electrons within the GeC_2P_2 fragment scaffold shows a high degree of electron delocalization on the surface of the *nido*-cluster (see the Supporting Information, section 9.7, Figure S58).

The cyclic voltammogram (CV; Figure 1e) of [Ge{η^4-**IDP**}]$^{2+}$ $[\mathbf{1}]^{2+}$ reveals two reversible and well-separated reduction waves [acetonitrile: $E_{1/2,1}$ = −1.27 V; $E_{1/2,2}$ = −1.60 V, 1,2-dimethoxyethane (DME): $E_{1/2,1}$ = −1.24 V; $E_{1/2,2}$ = −1.73 V, all potentials given vs. ferrocene/ferrocenium (Fc/Fc^+)]. UV/Vis spectro-electrochemical studies show that the one-electron reduction of $[\mathbf{1}]^{2+}$ proceeds cleanly via two isosbestic points indicating no further intermediates are involved in this process (see Supporting Information).

Accordingly, $[\mathbf{1}](BArF_{24})_2$ could be reduced with one equivalent of potassium graphite (KC_8) in DME whereby the deep orange radical cation [Ge{η^3-**IDP**}]$^{\bullet+}$ $[\mathbf{2}]^{\bullet+}$ is cleanly formed (Scheme 2b) and was isolated as the mixed salt $[\mathbf{2}](BArF_{24})$·$K(BArF_{24})$. The structure was determined by X-ray diffraction methods and a plot of $[\mathbf{2}]^{\bullet+}$ is shown in

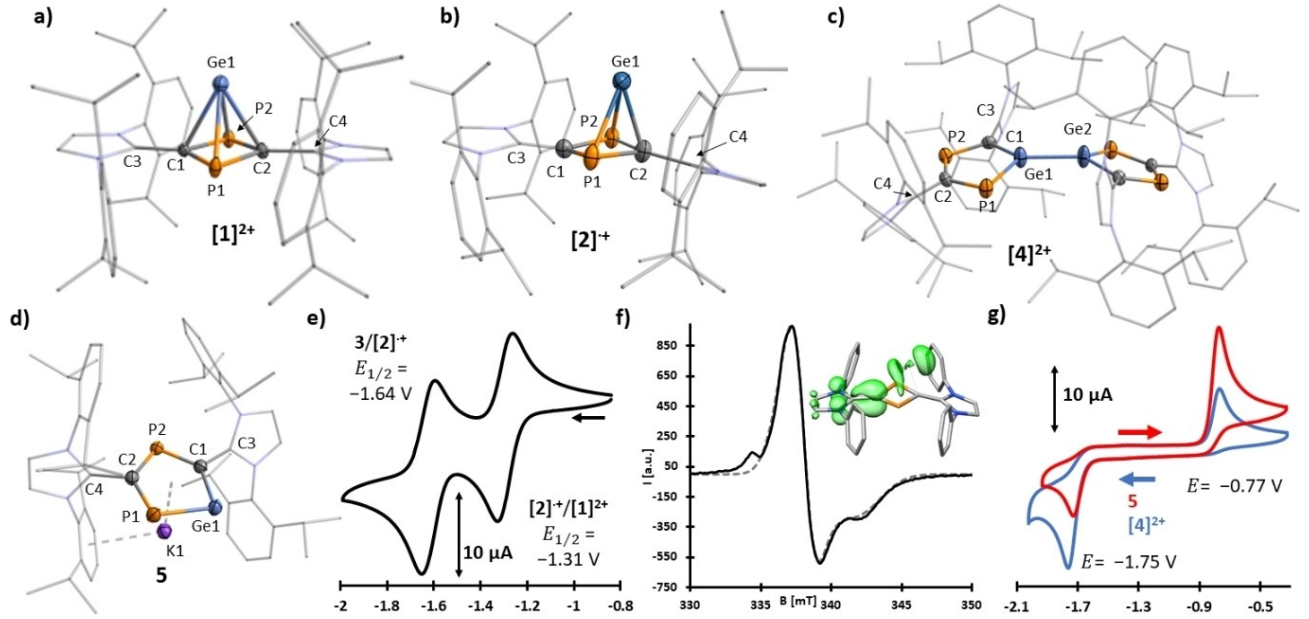

Figure 1. Molecular structures of [**1**]$(Ga_2Cl_7)(Ga_3Cl_{10})$ (a), [**2**]$(BArF_{24})$ (b), [**4**]$(BArF_{24})_2$ (c) and 5·K$(BArF_{24})$ (d) with ellipsoids at the 50% probability level. For clarity, in all cases only the cations are shown, hydrogens are omitted and IPr groups are drawn as transparent wireframes. For $[\mathbf{1}]^{2+}$, only one of two crystallographically independent cations in the asymmetric unit is shown; structural parameters of the second molecule are given in the Supporting Information. $[\mathbf{2}]^{\bullet+}$ and **5** are shown without disorder. Selected distances [Å] and angles [°] of $[\mathbf{1}]^{2+}$: Ge1–P1 2.452(1), Ge1–P2 2.441(2), Ge1–C1 2.280(4), Ge1–C2 2.265(4), C1–C3 1.441(5), C2–C4 1.438(6), P1–C1 1.803(4), P1–C2 1.807(4); $[\mathbf{2}]^{+}$: Ge1–P1 2.467(1), Ge1–P2 2.473(1), Ge1–C1 2.721(3), Ge1–C2 2.141(3), C1–C3 1.392(3), C2–C4 1.415(3), P1–C1 1.809(2), P1–C2 1.832(2); $[\mathbf{4}]^{2+}$: Ge1–Ge2 2.367(8), Ge1–P1 2.173(2), P1–C2 1.798(4), C2–P2 1.741(5), P1–C1 1.749(6), C1–Ge1 1.877(6), C1–C3 1.443(7), C2–C4 1.456(7), Σ_{Ge1} 358.8(3), Σ_{Ge2} 356.9(3), ∢(C_2P_2Ge) 25.7; $[5\cdot K]^{+}$: Ge1–P1 2.24 (1), P1–C1 1.802(9), C1–P2 1.731(2), P2–C2 1.745(2), C2–Ge1 1.978(4), C1–C3 1.455(3), C2–C4 1.443(3). e) CV of [**1**]$(BArF_{24})_2$ (all values vs. Fc/Fc^+, scan rate: 100 mV s^{-1}). The second scan is shown and the scan direction is indicated with an arrow. f) X-band EPR spectrum of [**2**]$(BArF_{24})\cdot K(BArF_{24})$ in the solid state and calculated spin-density of $[\mathbf{2}]^{\bullet+}$ (black: experimental data, dotted line: fitted spectrum). g) CV of $[\mathbf{4}]^{2+}$ (*blue* trace) and 5 (*red* trace) (scan rate: 100 mV s^{-1}). The second scan is shown and the scan directions are indicated with arrows..

Figure 1b. The long Ge–C1 distance [2.721(3) Å] indicates opening of the cluster framework and the germanium atom is η^3-coordinated by two P atoms and one C atom of the central C_2P_2 ring. The exocyclic bond between the non-coordinating carbon atom of the C_2P_2 ring and the respective IPr unit is slightly shorter [C1–C3 1.392(3) Å] than the other [C2–C4 1.415(3) Å]. The UV/Vis spectra of $[\mathbf{2}]^{\bullet+}$ match the spectra of species observed in the spectro-electrochemical studies of the one-electron reduction of $[\mathbf{1}]^{2+}$ introduced above, confirming the identity of the electrogenerated species (see the Supporting Information, Figure S17 and section 8). The EPR spectrum of $[\mathbf{2}]^{\bullet+}$ at 173 K in the solid-state reveals a rhombic signal with $g_x = 1.9733$, $g_y = 1.9984$ and $g_z = 2.0040$ (Figure 1f; for an EPR in DME solution at r.t. see the Supporting Information, section 5).

The g_{iso} value (1.992) is smaller than the one of the free electron (2.0023) indicating influence of the heavy germanium center via spin-orbit coupling.[27] A spin population of 0.34 e at the germanium center is calculated by DFT (see inset in Figure 1f, for details see the Supporting Information, section 5), while the majority of the spin population is distributed over C1 (0.26 e) and the attached IPr unit (0.32 e). In combination with the experimental data, these calculations show that $[\mathbf{2}]^{\bullet+}$ is best described by the mesomeric distonic radical cation structures **A** and **B**, with **A** as major contributor to the electronic ground state (Scheme 2b, see the Supporting Information, Figure S50).[28]

While [**2**](BArF24)·K(BArF24) is stable in the solid-state, it undergoes a structural rearrangement in solution: After ten days at ambient temperature in DME, the radical cation $[\mathbf{2}]^{\bullet+}$ has fully isomerized to the diamagnetic cherry-red species $[Ge_2C_4(IPr)_4P_4]^{2+}$ $[\mathbf{4}]^{2+}$ (Scheme 2b), which could be isolated in single-crystalline form as [**4**]$(BArF_{24})_2\cdot K(BArF_{24})_{1.8}$. A plot of the structure of $[\mathbf{4}]^{2+}$ is shown in Figure 1c. This dication is best characterized as a 1,1′-bis(2,4-diphosphagermolide) with two almost planar five-membered GeC_2P_2 rings [P2–C2–P1–Ge1: 1.6(3)°] linked via a rather short Ge–Ge single bond [2.367(8) Å]. All bond lengths within the GeC_2P_2 rings are in between the standard values expected for a single and a double bond and indicate delocalization of the π-electron system perpendicular to the ring planes (see caption of Figure 1). The two GeC_2P_2 rings are not coplanar and are tilted by 30° along the Ge–Ge axis. Again, the exocyclic C1–C3/C2–C4 bonds (Ø 1.45 Å) are relatively long and indicate imidazolium character for the IPr units. Formally, this places one negative charge on every GeC_2P_2 ring relating them to germole anions, $[GeC_4R_5]^-$.[29] However, while in these the Ge atom is typically located in a trigonal-pyramidal coordination sphere, thus rendering them only weakly aromatic, the sum of bond angles around the two germanium atoms Ge1 (359°) and Ge2 (357°) in $[\mathbf{4}]^{2+}$

indicates an almost ideal trigonal-planar environment. UV/Vis spectra in combination with TDDFT and CASSCF calculations (see the Supporting Information, section 9.5) allowed to characterize $[\mathbf{4}]^{2+}$ as an imidazolium-substituted digermole-diide with two aromatic 6π-electron GeC_2P_2 rings connected via the central Ge–Ge bond. The aromaticity of each GeC_2P_2 ring is indicated by the relatively large negative NICS(0) value of −10.2. Furthermore, the electron localization function of the π-electrons (ELF-π) within the GeC_2P_2 rings shows a high degree of delocalization (see the Supporting Information, section 9.7, Figure S59).[30] The delocalization was quantified by the aromatic fluctuation index FLU-π which lies well within the range reported for aromatic hydrocarbons (0.070).[31] In addition, the CASSCF orbitals and the ELF-π of $[\mathbf{4}]^{2+}$ show some minor π-overlap between the two Ge centers which might partially account for the rather short bond length.

While determined as a reversible redox couple by CV studies, spectro-electrochemical UV/Vis studies revealed that the product generated upon reduction of $[\mathbf{2}]^{\bullet+}$ at $E_{1/2,2} = -1.60$ V could not be isolated and observed in these experiments (see the Supporting Information, section 8), despite the transfer of ca. 1 equivalent of charge. Hypothesizing that the high ionic strength of the electrolysis solution is responsible for the instability of such resulting doubly reduced species, we investigated the stoichiometric two electron reduction of $[\mathbf{1}]^{2+}$.

When two equivalents of KC_8 or decamethylcobaltocene, $[Co(C_5Me_5)_2]$, are added as reductant to the dication $[\mathbf{1}]^{2+}$, a new product **3** is detected at low temperatures ($T = 235$ K) in toluene/acetonitrile (1:1) by $^{31}P\{^1H\}$ NMR spectroscopy (see the Supporting Information, section 7). The ^{31}P resonance signal at $\delta = 70$ ppm is broad ($\nu_{FWHM} = 1000$ Hz) indicating a dynamic phenomenon (likely a "flip-flop" movement of the Ge center between C1 and C2). By comparison with the calculated NMR shift (see the Supporting Information, section 9.3), a polyhedral structure comparable to the one of $[\mathbf{2}]^{\bullet+}$ is assigned to neutral [Ge{η³-IDP}] **3**. The calculated structure of **3** shows one short IPr–C bond with C=C double bond character and a Ge^{II} center, indicating that the two-electron reduction of $[\mathbf{1}]^{2+}$ takes place at this IPr moiety (Scheme 2, see the Supporting Information for details). This species cannot be isolated and rearranges to compound $GeC_2(IPr)_2P_2$ **5** as major product within 2 days. The latter compound is more conveniently synthesized by reduction of the bicyclic dication $[\mathbf{4}]^{2+}$ with two equivalents of KC_8 in acetonitrile in over 70 % isolated yield as deep red crystals of composition $\mathbf{5}\cdot K(BArF_{24})$. A plot of the structure of $[\mathbf{5}\cdot K]^+$ (determined by X-ray diffraction methods using a single crystal) is shown in Figure 1d.

The K^+ ion of the co-crystallized salt $K(BArF_{24})$ coordinates in an η⁵-fashion to the almost planar GeC_2P_2 ring (P2–C1–P1–Ge1: 5.3°). This feature is commonly seen in heteroatom-substituted anionic aromatic cyclopentadienides.[32] Again, the C1–C3/C2–C4 bonds are long (Ø 1.45 Å) indicating positively charged IPr groups connected to a formally dianionic GeC_2P_2 ring making **5** overall neutral. A possible Lewis-structure of **5** would therefore show two C=P double bonds and a $(Ge^{II})^{2-}$ center with two lone pairs of which one is located within and the other perpendicular to the ring plane. Hence, $GeC_2(IPr)_2P_2$ **5** is, according to the Hückel-rules, a 6π-electron configured 2D aromatic heterocycle. The highly deshielded ^{31}P resonances are in accordance with this assumption (P1: δ = 354.5 ppm; P2: δ = 310.5 ppm; $^2J_{PP} = 19$ Hz). Similarly to $[\mathbf{4}]^{2+}$, UV/Vis spectra together with TDDFT and CASSCF calculations indicate the presence of a 6π-system within the GeC_2P_2 ring in **5** (see the Supporting Information, section 9.6). The presence of an aromatic π-system is furthermore substantiated by the negative NICS(0) value of −7.5, the ELF-π (see the Supporting Information, Figure S59) and the FLU-π of 0.067.

One-electron oxidation of heterocycle **5** with the ferrocenium salt $[Fc](BArF_{24})$ gives the dimeric dication $[\mathbf{4}]^{2+}$, indeed. This in turn can be further oxidized with an excess of $Ag(SbF_6)$ to give the germapyramidane $[\mathbf{1}]^{2+}$. Alternatively, **5** can be oxidized to $[\mathbf{1}]^{2+}$ directly upon treatment with an excess of $Ag(SbF_6)$. These reactions close the synthetic cycle shown in Scheme 2. To the best of our knowledge, $[\mathbf{1}]^{2+}$ and the carborane **III** (see Scheme 1) are the only examples for a fully reversible redox cycle by which a 3D aromatic cluster is mutually converted to a 2D aromatic cycle.

But how does this profound structural rearrangement proceed? To gain insight into a possible reaction mechanism, further electrochemical studies were conducted (see the Supporting Information, section 8 for details). The CV of $[\mathbf{2}](BArF_{24})\cdot K(BArF_{24})$ is identical to the one of $[\mathbf{1}](BArF_{24})_2$, confirming that the isolated compound $[\mathbf{2}]^{\bullet+}$ is indeed the one-electron reduction product of $[\mathbf{1}]^{2+}$ observed in the CV studies (formed at $E_{1/2,1} = -1.27$ V). The CV of $[\mathbf{4}](BArF_{24})_2\cdot K(BArF_{24})_{1.8}$ and $\mathbf{5}\cdot K(BArF_{24})$ are particularly insightful: When the CV of $[\mathbf{4}]^{2+}$ is started with an oxidative scan [solvent: MeCN, electrolyte: nBu_4NPF_6], a quasi-reversible oxidation to the trication $[Ge_2C_4(IPr)_4P_4]^{3+}$ $[\mathbf{8}]^{3+}$ (Figure 2) is observed at 0.30 V (see the Supporting Information, Figure S37). In DFB, a second oxidative process, an irreversible oxidation at 1.1 V is observed (see the Supporting Information, Figure S41), which is assigned to the tetracation $[\mathbf{9}]^{4+}$ that deposits onto the electrode surface. The reductive scan shows an irreversible reduction wave with doubled current intensity at −1.75 V. Is the potential scan reversed after this irreversible two-electron reduction, an oxidation wave (irreversible up to scan rates of 500 mV s^{-1}) is observed at −0.77 V (see Figure S43 in the Supporting Information). The CV of **5** shows the same features already detected in the CV of the digermole $[\mathbf{4}]^{2+}$: An irreversible oxidation wave at $E_{red} = -0.77$ V is observed and after reversal of the potential, an irreversible reduction wave at −1.75 V is seen. The relative intensities of these processes, which are reversed in the case of **5**, together with the scan-rate dependence data, indicate the presence of EC mechanisms which involve the formation of the short-lived radical cations $[GeC_2(IPr)_2P_2]^{\bullet+}$ $[\mathbf{6}]^{\bullet+}$ and $[\mathbf{10}]^{\bullet+}$ resulting from the oxidation of **5** and the reduction of $[\mathbf{4}]^{2+}$ respectively, which conversely dimerize or disproportionate (see the Supporting Information, section 8.8). These data

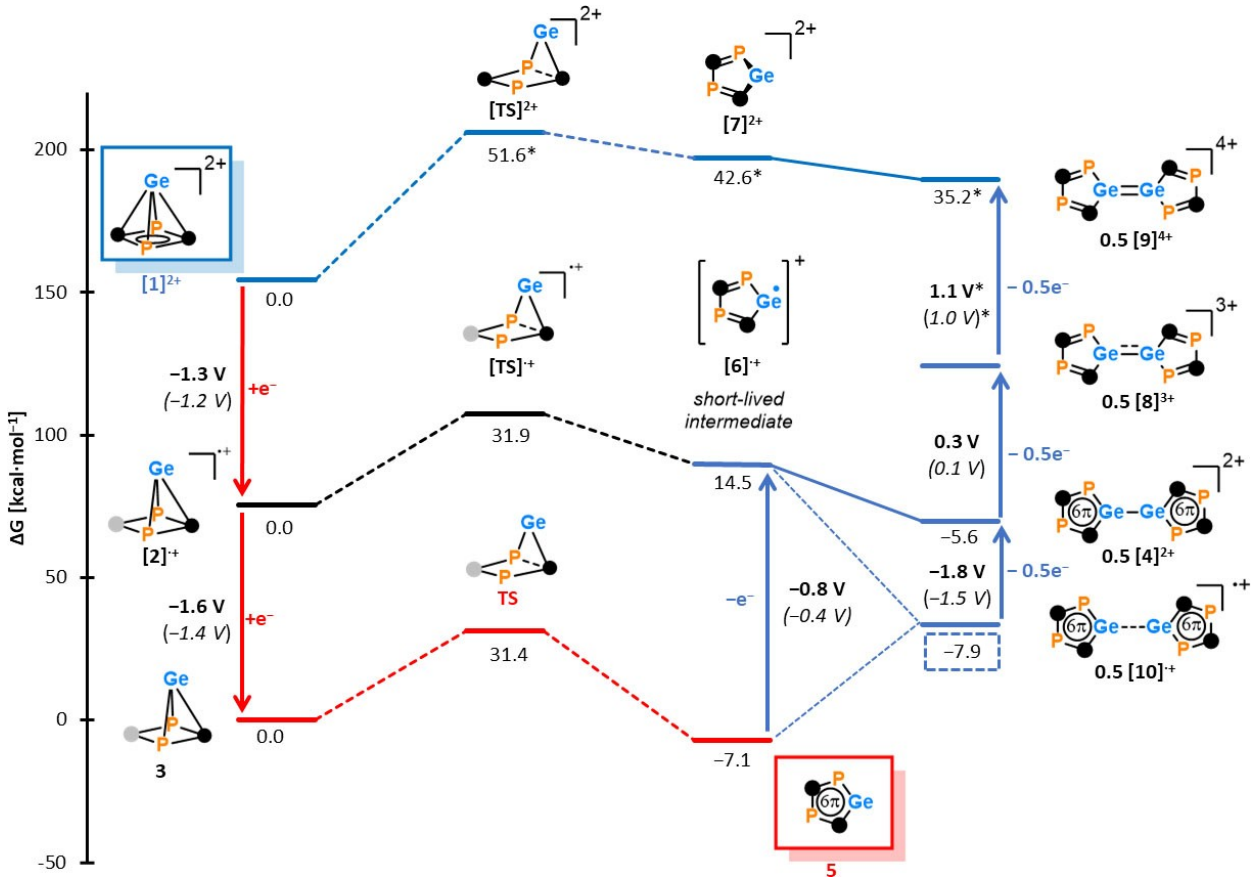

Figure 2. Calculated redox-cycle of $[\mathbf{1}]^{2+}$ (geometries and thermal corrections: B97-3c,[33] electronic energies: M06L-D3(0)/def2-TZVPP[34–37]). All potentials $E°_{calc}$ are given in V *vs.* the redox couple Fc/Fc^{+}. Experimentally determined potentials from CV studies are given in bold and calculated potentials are given in parentheses and italics. All values were obtained using a solvent model for acetonitrile, except for the ones marked with an asterisk, which were obtained using a solvent model for DFB. Black circles denote a carbon atom bearing a singly bound, cationic imidazolium moiety, while a grey circle denotes a multiply bonded carbene substituent.

are in good agreement with the rapid formation of the dimer $[\mathbf{4}]^{2+}$ upon oxidation of **5** and vice versa (vide infra).

DFT calculations using a truncated model where 2,6-diisopropylphenyl groups of IPr have been replaced by phenyl groups) allow to propose the mechanism shown in Figure 2. The reductive pathway $[\mathbf{1}]^{2+}+2\,e^{-}\rightarrow\mathbf{5}$ is depicted in red: In accordance with the observation of two reversible reduction waves in the CV of $[\mathbf{1}]^{2+}$, this *nido*-cluster is reduced stepwise by two electrons to give first the polyhedral radical cation $[\mathbf{2}]^{\bullet+}$ and then the cluster **3**. Subsequently, **3** rearranges to give **5** in an exothermic reaction $\Delta G_{calc}=-7.1\,kcal\,mol^{-1}$. The energy of the calculated activated complex at the transition state, **TS**, agrees with a slow rearrangement ($\Delta G^{\ddagger}_{calc}=31.4\,kcal\,mol^{-1}$). This mechanism corresponds to an electron transfer/ electron transfer/ chemical reaction (EEC) mechanism. Another possibility would be that already at the stage of the radical cluster cation $[\mathbf{2}]^{\bullet+}$ the rearrangement to the cyclic radial $[\mathbf{6}]^{\bullet+}$ takes place, which leads to the formation of $[\mathbf{4}]^{2+}$ (see the black pathway in Figure 2 and the Supporting Information, section 9.4 for the full mechanism). But the rather high activation barrier of $\Delta G^{\ddagger}_{calc}=31.9\,kcal\,mol^{-1}$ makes this process less likely.

The oxidative pathway $\mathbf{5}-\mathbf{2}\,e^{-}\rightarrow[\mathbf{1}]^{2+}$ is shown in blue. Based on the experiments and DFT calculations a more complex mechanism involving multiple (electro)chemical steps is proposed: In the first step, the neutral 6π-aromatic cycle $GeC_2(IPr)_2P_2$ **5** is oxidized at $E_{ox}=-0.77$ V ($E_{calc}=-0.4$ V) to the radical cation $[\mathbf{6}]^{\bullet+}$. Subsequently, this species could dimerize to $^{1}/_{2}$ $[(GeC_2(IPr)_2P_2)_2]^{2+}$ $[\mathbf{4}]^{2+}$ ($\Delta G_{calc}=-20.1\,kcal\,mol^{-1}$). The radical cation $[\mathbf{6}]^{\bullet+}$ shows significant calculated spin population at the Ge atom explaining the formation of a Ge–Ge bond during the dimerization process (see Figure S54 in the Supporting Information). Alternatively, $[\mathbf{6}]^{\bullet+}$ could also react with remaining **5** to yield the radical species $[\mathbf{10}]^{\bullet+}$according to the equation $\mathbf{5}-0.5\,e\rightarrow0.5\,\mathbf{5}+0.5\,[\mathbf{6}]^{\bullet+}\rightarrow0.5\,[\mathbf{10}]^{\bullet+}$ (process indicated with dotted lines in Figure 2, $\Delta G_{calc}=-7.9\,kcal\,mol^{-1}$). The radical cation $[\mathbf{10}]^{\bullet+}$ is then further oxidized at a rather low potential to yield $[\mathbf{4}]^{2+}$ ($E_{calc}=-1.5$ V). With the truncated DFT model, the dimerization of $[\mathbf{6}]^{\bullet+}$ as well as the formation of $[\mathbf{10}]^{\bullet+}$ proceeds barrier-less which is in qualitative agreement with the overall rapid formation of $[\mathbf{4}]^{2+}$ upon oxidation of **5** observed in CV studies. The digermole $[\mathbf{4}]^{2+}$ is subsequently oxidized in two consecutive one electron oxidations, firstly at $E_1=0.3$ V ($E_{calc}=0.1$ V) to give $[\mathbf{8}]^{3+}$ and, secondly, at

$E_2 = 1.1$ V ($E^2_{calc} = 1.0$ V) to the bicyclic tetracation $[(GeC_2(IPr)_2P_2)_2]^{4+}$ $[\mathbf{9}]^{4+}$. These calculations are in full agreement with the CV study of $[\mathbf{4}]^{2+}$ recorded in DFB (vide supra). Subsequently, $[\mathbf{9}]^{4+}$ dissociates in a weakly endothermic reaction ($\Delta G_{calc} = 7.4$ kcal mol^{-1}) to the monocylic dication $[GeC_2(IPr)_2P_2]^{2+}$ $[\mathbf{7}]^{2+}$ which easily rearranges exothermally ($\Delta G_{calc} = -42.6$ kcal mol^{-1}) into the *nido*-cluster $[\mathbf{1}]^{2+}$ via a small activation barrier of $\Delta G^{\neq}_{calc} = 9.0$ kcal mol^{-1}, thus closing the redox-cycle.

The interconversion of $[\mathbf{1}]^{2+}$ and **5** is not only of fundamental interest but is also interesting for the development of switchable materials: The cluster $[\mathbf{1}]^{2+}$ shows a small, calculated dipole moment of only 0.6 Debye which is directed from the midpoint of the C_2P_2 cycle to the Ge atom. On the other hand, heterocycle **5** shows a substantially larger dipole moment of 10.7 Debye which is flipped by 90° and is arranged in the plane of the ring (see Figure 3). A profound structural change of molecules provoked by physical stimuli is a prerequisite for the development of smart materials.[38–43] Presently, two main factors prevent the application of the actual redox pair $[\mathbf{1}]^{2+}$/**5** in such materials. First, the isomerization **3**→**5** has a significant kinetic barrier, and, secondly, the reoxidation process **5**→$[\mathbf{1}]^{2+}$ is only feasible with chemical oxidants, due to the instability of $[\mathbf{9}]^{4+}$ in electrochemical media (see above). Therefore, modifications of $[\mathbf{1}]^{2+}$ need to be investigated which overcome these drawbacks.

Conclusion

In summary, the combination of Ge, P and C as cluster atoms and imidazolium groups as substituents make the *nido*-cluster $[\mathbf{1}]^{2+}$ a unique species which allowed to study the rearrangement of a 3D 5-vertex cluster into a 2D cycle promoted by two-electron reduction. This transformation is reversible upon oxidation. Both, the two-electron reduction, and oxidation proceed stepwise in one electron transfer steps and the detection and isolation of intermediates makes it possible to propose a reaction mechanism. Notably, the reductive conversion proceeds on a different minimal energy reaction pathway (MERP) than the oxidative one.

The mutual conversion of a 3D cluster into a 2D cycle in a redox reaction is not only of fundamental value for the validity of concepts concerning structure and chemical bonding, but also may be of interest for applications as shown by the significant change in magnitude and direction of the dipole moments in $[\mathbf{1}]^{2+}$ and **5**. If pairs of redox active molecules related to $[\mathbf{1}]^{2+}$/**5** can be incorporated in a controlled manner into materials or arranged on surfaces, such phenomena may be used for molecular switches or optoelectronic devices, indeed.[44–47] In silico explorations of such redox pairs are underway in our laboratories.

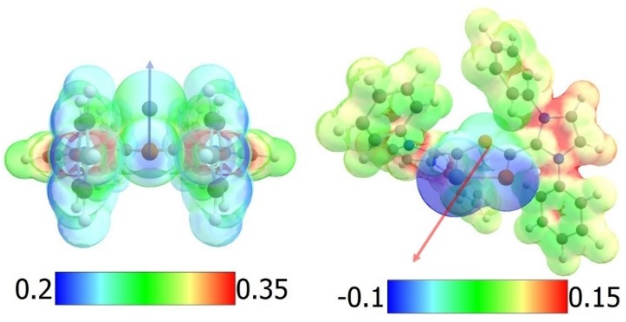

Figure 3. Electrostatic potential maps of $[\mathbf{1}]^{2+}$ and **5**. The direction of the dipole moment vector is indicated by an arrow.

Acknowledgements

We thank the Copéret group (ETH Zurich) for access and assistance with EPR spectroscopy. PC gratefully acknowledges funding by the Deutsche Forschungsgemeinschaft (DFG, grant 438203135). This work was supported by the ETH Zürich (grant ETH-36 17-2) and Swiss National Science Foundation (grant 20020 181966).

Conflict of Interest

The authors declare no conflict of interest.

Data Availability Statement

The data that support the findings of this study are available from the corresponding author upon reasonable request.

Keywords: Aromaticity · Cluster Compounds · Density Functional Calculations · Main-Group Elements · Redox Chemistry

[1] Y. Canac, G. Bertrand, *Angew. Chem. Int. Ed.* **2003**, *42*, 3578–3580; *Angew. Chem.* **2003**, *115*, 3702–3704.
[2] K. Wade, *J. Chem. Soc. Chem. Commun.* **1971**, 792–793.
[3] R. W. Rudolph, *Acc. Chem. Res.* **1976**, *9*, 446–452.
[4] D. M. P. Mingos, *Acc. Chem. Res.* **1984**, *17*, 311–319.
[5] E. Hückel, *Z. Phys.* **1931**, *70*, 204–286.
[6] S. Masamune, M. Sakai, H. Ona, A. J. Jones, *J. Am. Chem. Soc.* **1972**, *94*, 8956–8958.
[7] K. S. Kharnaior, A. K. Chandra, R. H. D. Lyngdoh, *J. Mol. Model.* **2021**, *27*, 218.
[8] W. D. Stohrer, R. Hoffmann, *J. Am. Chem. Soc.* **1972**, *94*, 1661–1668.
[9] M. Unverzagt, H.-J. Winkler, M. Brock, M. Hofmann, P. von Ragué Schleyer, W. Massa, A. Berndt, *Angew. Chem. Int. Ed. Engl.* **1997**, *36*, 853–855; *Angew. Chem.* **1997**, *109*, 879–882.
[10] V. Ya. Lee, H. Sugasawa, O. A. Gapurenko, R. M. Minyaev, V. I. Minkin, H. Gornitzka, A. Sekiguchi, *J. Am. Chem. Soc.* **2018**, *140*, 6053–6056.
[11] C. Balzereit, H.-J. Winkler, W. Massa, A. Berndt, *Angew. Chem. Int. Ed. Engl.* **1994**, *33*, 2306–2308; *Angew. Chem.* **1994**, *106*, 2394–2396.
[12] D. H. Evans, *Chem. Rev.* **2008**, *108*, 2113–2144.
[13] Z. Li, X. Chen, D. M. Andrada, G. Frenking, Z. Benkö, Y. Li, J. R. Harmer, C.-Y. Su, H. Grützmacher, *Angew. Chem. Int. Ed.* **2017**, *56*, 5744–5749; *Angew. Chem.* **2017**, *129*, 5838–5843.

[14] V. I. Minkin, R. M. Minyaev, G. V. Orlova, *J. Mol. Struct.* **1984**, *110*, 241–253.
[15] E. Lewars, *J. Mol. Struct.* **1998**, *423*, 173–188.
[16] E. Lewars, *J. Mol. Struct.* **2000**, *507*, 165–184.
[17] Deposition Numbers 2158484 ([**1**](Ga_2Cl_7)(Ga_3Cl_{10})), 2158485 (**[2]BArF$_{24}$**), 2158486 (**[4][BArF$_{24}$]$_2$**) and 21584847 (**5 KBArF$_{24}$**) contain the supplementary crystallographic data for this paper. These data are provided free of charge by the joint Cambridge Crystallographic Data Centre and Fachinformationszentrum Karlsruhe Access Structures service.
[18] M. D. Francis, P. B. Hitchcock, *Chem. Commun.* **2002**, 86–87.
[19] M. D. Francis, P. B. Hitchcock, *Organometallics* **2003**, *22*, 2891–2896.
[20] V. Ya. Lee, Y. Ito, A. Sekiguchi, H. Gornitzka, O. A. Gapurenko, V. I. Minkin, R. M. Minyaev, *J. Am. Chem. Soc.* **2013**, *135*, 8794–8797.
[21] V. Y. Lee, Y. Ito, O. A. Gapurenko, A. Sekiguchi, V. I. Minkin, R. M. Minyaev, H. Gornitzka, *Angew. Chem. Int. Ed.* **2015**, *54*, 5654–5657; *Angew. Chem.* **2015**, *127*, 5746–5749.
[22] V. Y. Lee, H. Sugasawa, O. A. Gapurenko, R. M. Minyaev, V. I. Minkin, H. Gornitzka, A. Sekiguchi, *Chem. Eur. J.* **2016**, *22*, 17585–17589.
[23] K. M. Baines, W. G. Stibbs, *Coord. Chem. Rev.* **1995**, *145*, 157–200.
[24] F. H. Allen, O. Kennard, D. G. Watson, L. Brammer, A. G. Orpen, R. Taylor, *J. Chem. Soc. Perkin Trans. 2* **1987**, S1–S19.
[25] D. A. Pantazis, J. E. McGrady, J. M. Lynam, C. A. Russell, M. Green, *Dalton Trans.* **2004**, 2080–2086.
[26] J. Poater, C. Viñas, I. Bennour, S. Escayola, M. Solà, F. Teixidor, *J. Am. Chem. Soc.* **2020**, *142*, 9396–9407.
[27] W. D. Woodul, E. Carter, R. Müller, A. F. Richards, A. Stasch, M. Kaupp, D. M. Murphy, M. Driess, C. Jones, *J. Am. Chem. Soc.* **2011**, *133*, 10074–10077.
[28] X. Chen, L. L. Liu, S. Liu, H. Grützmacher, Z. Li, *Angew. Chem. Int. Ed.* **2020**, *59*, 23830–23835; *Angew. Chem.* **2020**, *132*, 24038–24043.
[29] P. von Ragué Schleyer, H. Jiao, B. Goldfuss, P. K. Freeman, *Angew. Chem. Int. Ed. Engl.* **1995**, *34*, 337–340; *Angew. Chem.* **1995**, *107*, 332–335.
[30] J. Poater, M. Duran, M. Solà, B. Silvi, *Chem. Rev.* **2005**, *105*, 3911–3947.
[31] E. Matito, M. Duran, M. Solà, *J. Chem. Phys.* **2005**, *122*, 014109.
[32] Z. Dong, M. Schmidtmann, T. Müller, *Chem. Eur. J.* **2019**, *25*, 10767–10767.
[33] J. G. Brandenburg, C. Bannwarth, A. Hansen, S. Grimme, *J. Chem. Phys.* **2018**, *148*, 064104.
[34] Y. Zhao, D. G. Truhlar, *Chem. Phys. Lett.* **2011**, *502*, 1–13.
[35] F. Weigend, R. Ahlrichs, *Phys. Chem. Chem. Phys.* **2005**, *7*, 3297–3305.
[36] S. Grimme, J. Antony, S. Ehrlich, H. Krieg, *J. Chem. Phys.* **2010**, *132*, 154104.
[37] S. Grimme, S. Ehrlich, L. Goerigk, *J. Comput. Chem.* **2011**, *32*, 1456–1465.
[38] M. Tasić, J. Ivković, G. Carlström, M. Melcher, P. Bollella, J. Bendix, L. Gorton, P. Persson, J. Uhlig, D. Strand, *Nat. Commun.* **2022**, *13*, 860.
[39] J. D. Harris, M. J. Moran, I. Aprahamian, *Proc. Natl. Acad. Sci. USA* **2018**, *115*, 9414–9422.
[40] M. Baroncini, L. Casimiro, C. de Vet, J. Groppi, S. Silvi, A. Credi, *ChemistryOpen* **2018**, *7*, 169–179.
[41] S. Erbas-Cakmak, D. A. Leigh, C. T. McTernan, A. L. Nussbaumer, *Chem. Rev.* **2015**, *115*, 10081–10206.
[42] S. Kassem, T. van Leeuwen, A. S. Lubbe, M. R. Wilson, B. L. Feringa, D. A. Leigh, *Chem. Soc. Rev.* **2017**, *46*, 2592–2621.
[43] D. Xiang, X. Wang, C. Jia, T. Lee, X. Guo, *Chem. Rev.* **2016**, *116*, 4318–4440.
[44] J. Lin Zhang, J. Qiang Zhong, J. Dan Lin, W. Ping Hu, K. Wu, G. Qin Xu, A. T. S. Wee, W. Chen, *Chem. Soc. Rev.* **2015**, *44*, 2998–3022.
[45] L. Gerhard, K. Edelmann, J. Homberg, M. Valášek, S. G. Bahoosh, M. Lukas, F. Pauly, M. Mayor, W. Wulfhekel, *Nat. Commun.* **2017**, *8*, 14672.
[46] A. Melloni, R. Rossi Paccani, D. Donati, V. Zanirato, A. Sinicropi, M. L. Parisi, E. Martin, M. Ryazantsev, W. J. Ding, L. M. Frutos, R. Basosi, S. Fusi, L. Latterini, N. Ferré, M. Olivucci, *J. Am. Chem. Soc.* **2010**, *132*, 9310–9319.
[47] N. Xin, J. Guan, C. Zhou, X. Chen, C. Gu, Y. Li, M. A. Ratner, A. Nitzan, J. F. Stoddart, X. Guo, *Nat. Rev. Phys.* **2019**, *1*, 211–230.

Manuscript received: August 9, 2022
Accepted manuscript online: September 24, 2022
Version of record online: October 21, 2022